

# Crystal fractionation, magma step ascent, and syn-eruptive mingling: the Averno 2 eruption (Phlegraean Fields, Italy)

Céline Fourmentraux · Nicole Métrich ·  
Antonella Bertagnini · Mauro Rosi

Received: 26 July 2010 / Accepted: 20 January 2012 / Published online: 7 February 2012  
© Springer-Verlag 2012

**Abstract** The 3.7 ka year-old Averno 2 eruption is one of the rare eruptions to have occurred in the northwest sector of the Phlegraean Fields caldera (PFC) over the past 5 ka. We focus here on the fallout deposits of the pyroclastic succession emplaced during this eruption. We present major and trace element data on the bulk pumices, along with major and volatile element data on clinopyroxene-hosted melt inclusions, in order to assess the conditions of storage, ascent, and eruption of the feeding trachytic magma. Crystal fractionation accounts for the evolution from trachyte to alkali-trachyte magmas; these were intimately mingled (at the micrometer scale) during the climactic phase of the eruption. The Averno 2 alkali trachyte represents one of the most evolved magmas erupted within the Phlegraean Fields area and belongs to the series of differentiated trachytic magmas erupted at different locations 5 ka ago. Melt inclusions record significant variations in H<sub>2</sub>O (from 0.4 to 5 wt%), S (from 0.01 to 0.06 wt%), Cl (from 0.75 up to 1 wt%), and F (from 0.20 to >0.50 wt%) during both magma

crystallization and degassing. Unlike the eruptions occurring in the central part of the PFC, deep-derived input(s) of gas and/or magma are not required to explain the composition of melt inclusions and the mineralogy of Averno 2 pumices. Compositional data on bulk pumices, glassy matrices, and melt inclusions suggest that the Averno 2 eruption mainly resulted from successive extrusions of independent magma batches probably emplaced at depths of 2–4 km along regional fractures bordering the Neapolitan Yellow Tuff caldera.

**Keywords** Phlegraean Fields · Averno 2 · Melt inclusions · Volatiles · Trachyte

## Introduction

Located in the Campanian Plain, along the Tyrrhenian margin of the Southern Apennines (Italy), the Phlegraean Fields is an active volcanic area dominated by a 12-km-wide nested caldera. The Phlegraean Fields caldera (PFC) results from successive collapses related to the eruption of the Campanian Ignimbrite (CI:  $39.3 \pm 0.1$  ka; De Vivo et al. 2001) and Neapolitan Yellow Tuff (NYT:  $14.9 \pm 0.4$  ka; Deino et al. 2004; Orsi et al. 1996). The CI and NYT units are both thought to be the residual portions of older large-volume magma reservoirs generated 60 and 15 ka ago, respectively (Pappalardo et al. 1999). In the last 15 ka, volcanic activity has mainly been confined to the PFC system (Fig. 1a), in which three main eruptive periods occurred successively (1) 15–9.5 ka ago, (2) 8.6–8.2 ka ago, and (3) 4.8–3.8 ka ago (Di Vito et al. 1999; Pappalardo et al. 2002; Orsi et al. 2004; Mastrolorenzo and Pappalardo 2006). The PFC system is one of the most dangerous volcanic complexes on Earth, owing to the

Communicated by G. Moore.

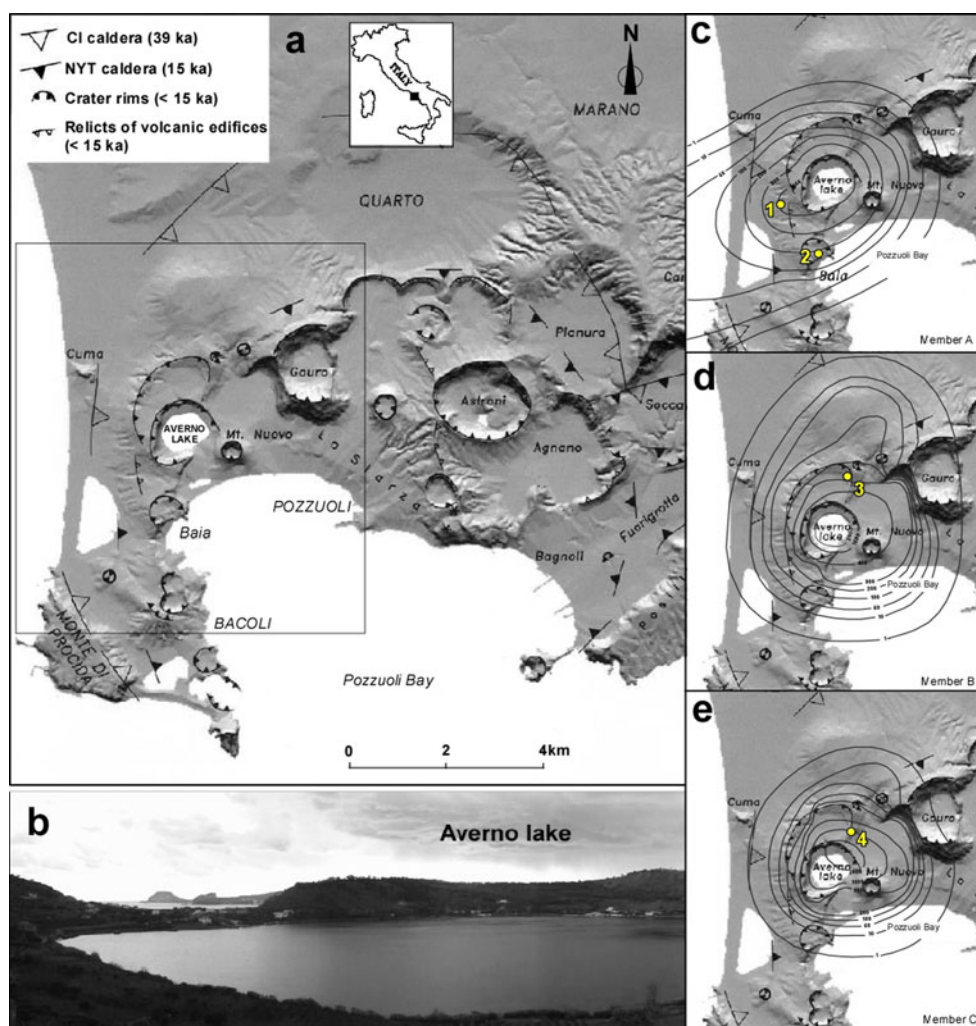
**Electronic supplementary material** The online version of this article (doi:10.1007/s00410-012-0720-1) contains supplementary material, which is available to authorized users.

C. Fourmentraux · N. Métrich · A. Bertagnini (✉)  
Istituto Nazionale di Geofisica e Vulcanologia, Sezione di Pisa,  
via della Faggiola, 32, 56126 Pisa, Italy  
e-mail: bertagnini@pi.ingv.it

C. Fourmentraux · M. Rosi  
Dipartimento di Scienze della Terra, Pisa, Italy

N. Métrich  
Institut de Physique du Globe, Sorbonne Paris Cité, UMR-CNRS  
7154, Université Paris Diderot, 75005 Paris, France

**Fig. 1** **a** Structural sketch map of the Phlegraean Fields caldera (PFc) (modified after Isaia et al. 2004). **b** View of Lake Averno. **c–e** Maps showing the total thickness (cm) distribution of members A, B, and C of the deposits from the Averno 2 eruption (modified after Di vito et al. 2010) and sample location. Numbers in plots 1c–e refer to the names of the stratigraphic sections: 1. Torretta (A0), 2. Amministratore (A2b and A2t), 3. Monte Russo (Bt), and 4. La Schiana (Cmb)



intense urbanization within the caldera and in its surroundings. Still active fumaroles and hot springs are widespread. Since 2000, soil degassing of deep-derived  $\text{CO}_2$  at the Solfatara fumarolic field has increased and has been associated with ground deformation and seismicity (Allard et al. 1991; Caliro et al. 2007; Chiodini and Frondini 2001; Chiodini et al. 2010). Unrest events (bradyseism) have affected the area in the last 35 years (e.g., Barberi et al. 1989); the last bradyseism episode occurred in the 1980s, resulting in a net 3.5 m uplift at Pozzuoli harbor (Orsi et al. 2004; De Natale et al. 2006). According to geodetic data, the 1982–1984 unrest may have been related to shallow magma intrusion (Amoruso et al. 2008), followed by upstreaming of magmatic  $\text{CO}_2$ -rich gas and low-pressure accumulation of mixed magmatic and hydrothermal components (Arienzo et al. 2010; Caliro et al. 2007). The existence of magma reservoir(s) at a depth of  $\sim 4$ –5 km was previously suggested on the basis of thermal (Wohletz et al. 1999), magnetic (Orsi et al. 1999), and seismological data (Ferrucci et al. 1992). More recently, seismic discontinuities detected at depths of 2.7

and 7.5 km were ascribed to the presence of a gas-bearing fractured rock layer overlying a low velocity zone with ponded partial melts (Zollo et al. 2008). The development of a mid-crustal sill-like magma reservoir, as hypothesized from seismic reflection profiles, is consistent with the magma crystallization pressure ( $\sim 200$  MPa) derived from petrological data on the Minopoli 2 eruption (10.2 ka; Mangiacapra et al. 2008) and the 39 ka year-old CI trachytic magma (Marianelli et al. 2006). It has been suggested (D'Antonio et al. 1999) that smaller, possibly shallower magma pockets fed the eruptions that took place in the PFc system over the past 12 ka. Recent seismic tomography studies did not detect magma pockets at depths shallower than 4 km (Zollo et al. 2008).

Magma evolution within the shallow portions of the PFc magmatic system has been ascribed to several processes: fractional crystallization (Armienti et al. 1983), mixing and/or mingling (e.g., Civetta et al. 1997; D'Antonio et al. 1999), and subordinate contamination (e.g., Pappalardo et al. 1999; Tonarini et al. 2004; Arienzo et al. 2009). More importantly,  $\text{CO}_2$ -rich gas influx



was recently suggested to play an effective role in triggering explosive eruptions (Mangiaccapra et al. 2008; Arienzo et al. 2010).

The Averno 2 eruption (3.7 ka BP according to Alessio et al. 1971) together with an older accretionary lapilli-rich ash bed (Averno 1, 4.5 ka according to Di Vito et al. 1999) and the neighboring Mt. Nuovo tuff cone dated to 1558 AD (Troise et al. 2007; D’Orlando et al. 2005) are the only examples of volcanic activity within the northwestern sector of the PFC over the past 5 ka. The Averno 2 eruption produced a well-exposed succession of pyroclastic deposits (Rosi and Sbrana 1987; Mastrolorenzo 1994; Di Vito et al. 1999, 2010) that provide an opportunity to decipher the processes governing the evolution of the youngest magma pockets.

We present here a systematic study of (1) the major and trace element geochemistry of bulk rocks and their glassy matrices representative of the Averno 2 fallout episodes, which complement recent literature data (Di Vito et al. 2010), and (2) major and volatile elements ( $H_2O$ , S, Cl, and F) in clinopyroxene-hosted melt inclusions. Melt inclusions in sanidine (the most abundant mineral phase) are cryptocrystalline, contain large bubbles and are not suitable for analysis. We provide melt entrapment pressures and a comprehensive scheme of the pressure-related evolution of volatiles in the general framework of the evolution of Phlegraean Fields magma.

## Volcanological background and sampling

The Averno 2 eruption took place at the intersection of NE–SW and NW–SE fault systems bordering the resurgent block of the NYT caldera (Orsi et al. 2004). Averno was possibly active at the same time as La Solfatara in the NE sector (Isaia et al. 2009). The eruption built up a 100-meter-high pyroclastic ring with a roughly circular crater filled by a 34-m-deep lake (Fig. 1b). This event was of moderate magnitude relative to the 4.1 ka old Agnano Monte Spina (AMS) Plinian eruption, with a total volume of erupted magma of about  $0.07 \text{ km}^3$  (DRE) (Di Vito et al. 2010).

The Averno 2 sequence, of which the stratigraphy is detailed in Di Vito et al. (2010), consists of fallout and surge deposits and is divided into three members named A through C, from the base to the top. In this work, only the fallout deposits were sampled at four different sites located 1–1.5 km from the vent (Fig. 1c). Member A is composed of six main pumice fall deposits alternating with minor thin ash-rich surge beds (Fig. 2a, b). We collected samples from 82-cm thick layer A0 (sample A0) at Torretta (Fig. 2a) and from the base and top of 70-cm thick layer A2 (samples A2b and A2t; Fig. 2b). According to Di Vito et al. (2010), the A2 sub-member was emplaced during the eruption climax that produced an estimated column height of 10 km, with a mass discharge rate of  $3.2 \cdot 10^6 \text{ kg/s}$ . Samples

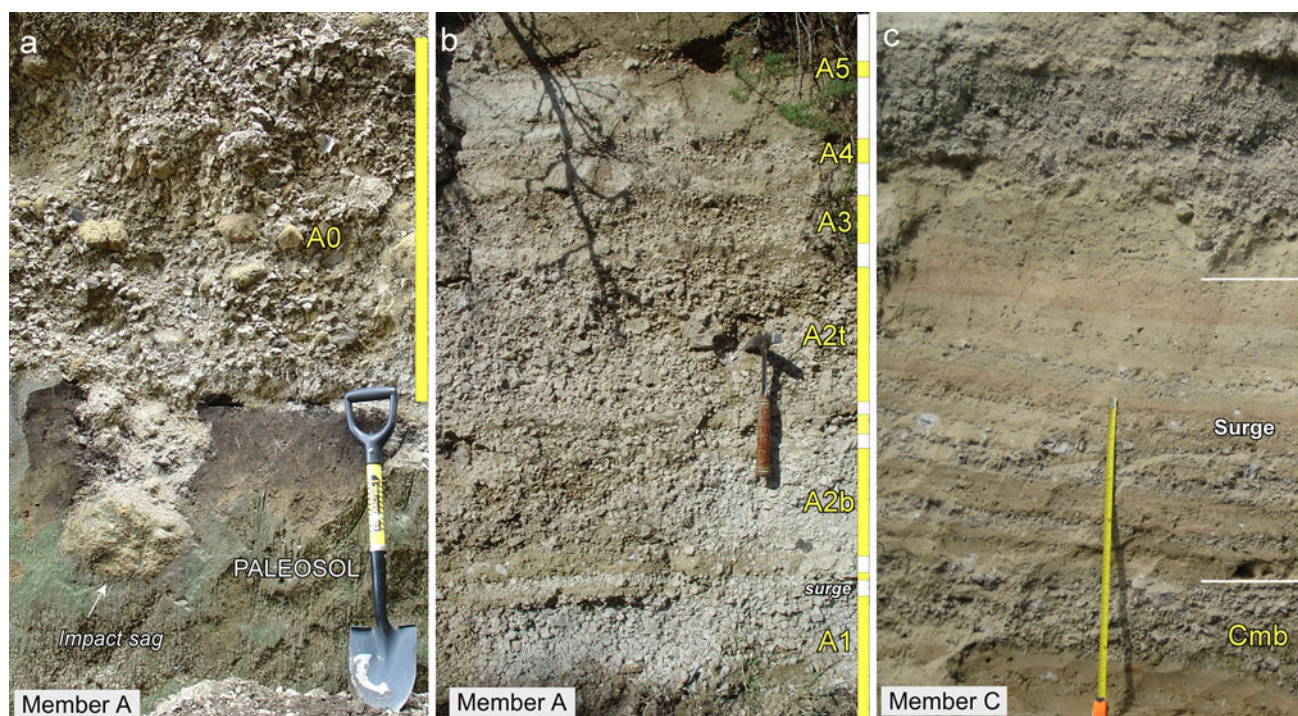


**Fig. 2** Snapshots of the Averno 2 deposits: **a** coarse-grained fallout bed (A0); **b** A1–A5 fallout deposits intercalated in minor surge beds (s); **c** Member C dominated by a surge sequence with a subordinate fallout bed

Bt and Cmb (Fig. 2c) are pumice clasts from 13- and 19-cm thick fallout layers in the upper portion of member B and in the middle portion of member C, respectively.

### Sample preparation and analytical procedures

Samples (A0, A2b, A2t, Bt, and Cmb) for bulk rock analysis were cleaned, washed in distilled water, crushed, and finely ground in an agate mill. Dm-sized bombs (3, 4) from each sampled layer were crushed, except for sample A2t, which was found to be heterogeneous. For this specific sample, four distinct dm-sized clasts were analyzed individually.

Major, minor, and trace elements were measured (Code 4Lithoresearch; <http://www.actlabsint.com>) at the Activation Laboratories Ltd (Ancaster, Canada): major elements using Inductively Coupled Plasma Optical Emission Spectroscopy (ICP-OES), trace elements and REE using Inductively Coupled Plasma Mass Spectrometry (ICP-MS). Chlorine was analyzed by instrumental neutron activation and F using a specific ion electrode.

The crystal content was determined in the five fallout samples of the Averno 2 sequence. For each sample, ~20 pumice clasts ranging from ~5 to 7 cm in diameter were crushed into <2-mm fragments and sieved. The 0.25–2-mm grain fraction was then immersed in a solution of fluoroboric acid (48 wt% solution in water) for about 3 h. After glass dissolution, crystals were dried and weighed in order to assess their proportion in each sample. Clinopyroxene crystals (110) were also hand-picked from the same samples under a binocular microscope in the 0.5–1-mm grain size fraction and double-face polished for melt inclusion study.

Melt inclusions were analyzed using a CAMECA SX50 electron microprobe (Camparis, Jussieu, France). Major element concentrations were measured with a 10 nA beam current, a counting time of 10–25 s, and a 10 µm defocused spot to minimize the loss of Na that was analyzed first with Si. A minimum of four spots were analyzed per melt inclusion and averaged. Analytical reliability was controlled against a reference glass: trachyte obsidian (CFA47) from the Phlegraean Fields (Métrich and Clocchiatti 1989). Minor elements (P, S, Cl, and F) were measured using a 30 nA beam current, a 15 µm spot size, and a peak counting time of 140 s. Two coupled TAP crystal analyzers were used to determine fluorine contents. Calibration was performed against reference silicic glass standards: a rhyolite (VNM50, F = 940 ppm), a trachyte (CFA47, F = 2,000 ppm), and a pantellerite (Ke12, F = 4,250 ppm) (Mosbah et al. 1991; Spilliaert et al. 2006). Under these analytical conditions, the relative error in Cl and F determinations was, respectively, 5 and 10%.

To avoid water loss, H<sub>2</sub>O concentrations were determined prior to electron probe analyses using a Nicolet Magna-IR 550 Fourier-transform infrared spectrometer (Saclay, France) equipped with a globar source a MCT/A detector, a KBr-XT beam splitter, and coupled with a Spectra-Tech microscope. Broadband absorbance at 3,535 cm<sup>-1</sup> was measured after curved baseline subtraction. Concentrations (*C*, wt%) were calculated according to Beer-Lambert's law as  $C = (M \times A) / (e \times \rho \times \epsilon)$ , where *A* is the absorbance and *M* the molar mass of the species (g mol<sup>-1</sup>). The molar absorptivity ( $\epsilon = 62 \text{ L mol}^{-1} \text{ cm}^{-1}$ ) and glass densities (from 2.40 to 2.44 g cm<sup>-3</sup>) are from Di Matteo et al. (2004). The sample thickness, varying from 15 to 63 µm, was accurately determined ( $\pm 3 \mu\text{m}$ ) by repeated measurement under the microscope. The analytical error in H<sub>2</sub>O measurements (3–4 times) is estimated to be  $\pm 10\%$ . Carbon was not detected, neither as molecular CO<sub>2</sub> nor as carbonates.

Phenocrysts were analyzed using EDAX X-4I on a Philips XL30 scanning electron microscope at the Dipartimento di Scienze della Terra (Pisa, Italy). A total of 100 juvenile pumice fragments were also separated from the 1.4–2 mm and 4–8 mm fractions of samples A0, A2b, A2t, Bt, and Cmb. They were repeatedly analyzed (a total of 164 analyses) in order to test their homogeneity. Backscattered electron (BSE) imaging allowed us to verify that the pumice matrices were microlite-free. Analytical conditions were 20 keV accelerating voltage, 0.1 nA beam current, and a working distance of 10 mm. We used a raster window of about  $10 \times 10 \mu\text{m}^2$  to avoid Na migration under the electron beam during analysis. A diopside and the CFA47 trachytic glass were used as internal standards (Electronic appendices 1 and 2). Halogen (Cl, F), S, and P were analyzed in glass fragments selected on the basis of the SEM dataset using an SX50 electron probe at the analytical conditions described for melt inclusions. Apatite crystals were also analyzed using an SX50 electron probe to determine major and trace element contents under the same analytical conditions described previously.

### Texture and chemical composition of Averno products and minerals

#### Bulk pumices

We report here the main textural features of coarse juvenile samples from the base (A0, A2b, and A2t), the middle (Bt), and the top (Cmb) of the Averno 2 sequence; these are described in detail elsewhere (Fourmentraux 2009). Juvenile clasts show fairly large variability in density, vesicularity, and texture. Three main types of clasts were



observed: (1) low-density, light-colored, microvesicular, and microlite-free clasts that were analyzed for major elements, P, S, Cl, and F, (2) high-density, dark-brown, microlite-rich clasts, and (3) banded clasts consisting of mm-thick stripes of types (1) and (2).

As a whole, the Averno pumices contain few crystals: contents vary from 0.2 to ~1 wt% in the pumice of Member A and reach 4 wt% in those of intermediate Member B and upper Member C, which often contains crystal aggregates and K-feldspar clusters. Averno pumices display an alkali-trachyte composition, as defined on the basis of the differentiation index (D.I. from 91 and 87) and the normative nepheline content (4–7 wt%) (Table 1). The base samples (A0, A2b, and A2t) have a peralkaline affinity, with an agpaitic index  $[(\text{Na}_2\text{O} + \text{K}_2\text{O})/\text{Al}_2\text{O}_3]$  of 0.98–0.96 (Table 1). The Averno 2 sequence is thus chemically zoned from nearly peralkaline trachyte to alkali trachyte, in agreement with previous studies (Rosi and Sbrana 1987; Civetta et al. 1988; Di Vito et al. 2010). Averno 2 pumices also show significant variations in highly incompatible elements such as Th (94.9–42.8 ppm), Ta (8.2–3.9 ppm), and As (72–34 ppm) and in HFSE, which define positive correlations passing through 0 (Fig. 3a, c). In contrast, V, Co, and Ba are significantly fractionated as differentiation progresses (Fig. 3e, g). In each diagram, the A2t sample displays a bimodal composition, testifying to the syn-eruptive mingling of two magma batches forming the fallout deposits of the base (A0) and the top (Cmb) of the sequence, respectively. This feature is further confirmed by SEM analysis of individual glassy shards (Electronic Appendix 2).

Fluorine is positively correlated with Th, and its bulk distribution coefficient ( $D_F$ ) is 0.25, as derived from the Rayleigh distillation law (Fig. 3d). In contrast, Cl behaves as a moderately compatible element ( $D_{\text{Cl}} = 0.9$ ; Fig. 3h) possibly due to its partitioning into the mineral or gas phases. On the basis of Th and  $\text{P}_2\text{O}_5$  contents in the bulk rocks, we estimate that the crystallization of only 0.003 wt% apatite would have removed ~840 ppm F and 350 ppm Cl from the melt. The effect of apatite crystallization on halogens dissolved in the trachytic melt is thus limited, implying that Cl is dominantly buffered by the gas phase, as explained later. Lastly, all samples display similar REE patterns, LREE enrichment ( $\text{La/Yb} = 23\text{--}24$ ), and a pronounced negative Eu anomaly (Fig. 4). The simultaneous lowering of the  $\text{K}_2\text{O}$  content (from 8.5 to 7 wt%) and  $\text{Eu}/\text{Eu}^*$  ratio (from 0.6 to 0.4) in the more differentiated terms reflects K-feldspar fractionation. Similar features have been previously described for the Campanian Ignimbrite, although Averno pumices display an even more evolved trachytic composition since their Zr/Sr ratio varies from 90 to 100 against <0.1–45 in CI samples (Civetta et al. 1997).

## Minerals

The mineral assemblage consists of dominant sanidine with subordinate amounts of clinopyroxene and plagioclase (Supplementary material 1), whereas biotite, apatite, and iron oxides represent only accessory minerals, in agreement with data from the literature (Di Vito et al. 2010). Sanidine compositions vary from  $\text{Or}_{63}$  to  $\text{Or}_{80}$ , but each individual crystal is homogeneous, as revealed by BSE imaging; the highest value ( $\text{Or}_{80}$ ) was found in the last eruptive products (Cmb). The composition of plagioclase ranges from bytownite ( $\text{An}_{80}$ ) to oligoclase ( $\text{An}_{30}$ ), with no zoning, but plagioclase ( $\text{An}_{45\text{--}80}$ ) preferentially occur in Cmb samples. Plagioclase frequently shows corroded cores ( $\text{An}_{45\text{--}41}$ ) mantled by sanidine ( $\text{Or}_{68\text{--}76}$ ), i.e., the so-called anti-rapakivi texture commonly described in trachytes from the Phlegraean Fields (e.g., Armienti et al. 1983; D’Orsano et al. 2005). Clinopyroxene spans a compositional range from Mg-rich diopside ( $\text{Wo}_{47}$ ,  $\text{En}_{49}$ ,  $\text{Fs}_5$ ) to hedenbergite ( $\text{Wo}_{48}$ ,  $\text{En}_{21}$ ,  $\text{Fs}_{31}$ ), with the Fe richest one ( $\text{Fs}_{11\text{--}31}$ ) in A0 pumices (Fig. 5). Clinopyroxenes showing oscillatory zoning and Mg-rich diopside or Fe-rich resorbed cores are uncommon. Biotite occurs as rare isolated crystals and in crystal aggregates with clinopyroxene and sanidine. Fluorapatite is frequently found as solid inclusions in clinopyroxene and more rarely as discrete phenocrysts in the most evolved terms (A0 and A2). It is slightly zoned with F contents varying from 2.4 to 2.8 and from 2.8 to 3.2 wt% in samples Cmb and Bt, respectively; Cl concentrations in the same samples range from 0.72 to 0.75 and from 0.74 to 0.67 wt%, respectively.

## Pumice matrices and melt inclusions

In each fallout deposit, the glassy matrices of the light-colored, microvesicular, microlite-free pumice clasts display a compositional range from the base to the top of the sequence (Fig. 6a), which matches that of the bulk rocks (Tables 1 and 2). This observation is in agreement with the low quantity of crystals in the pumice. In samples A0, A2b, and Cmb, the average composition of each set of matrices is very homogeneous (Table 2). The glassy matrices of pumices A0 and A2b have an alkali-trachyte composition ( $\text{K}_2\text{O} \sim 7$  wt%), whereas those of the top Cmb samples are slightly less evolved ( $\text{K}_2\text{O} \sim 8.5$  wt%), as are the bulk pumices and the obsidian clasts. In contrast, A2t matrices are heterogeneous at the micrometer scale, as revealed by SEM analysis of 40 individual clasts from the 1–2- and 4–8-mm grain size fractions (Electronic appendix 2). Their compositional bimodality ( $\text{K}_2\text{O} = 8.3 \pm 0.1$  and  $7.0 \pm 0.2$  wt%; Fig. 6a and Table 2) is in keeping with that of the bulk clasts. However, note that the dominant composition of the bulk rocks and that of their matrices are closely similar to the

**Table 1** Major oxide and trace element compositions of the Averno 2 bulk rocks

Member Sample Location	A A0 1-Torreta	A A2b 2-Amm.	A A2t 2-Amm.	A A2t 2-Amm.	Bt Bt 3-Mte Russo	Cmb Cmb 4-La Schiana
SiO <sub>2</sub> (wt%)	60.43	59.89	60.27	59.79	59.36	59.12
TiO <sub>2</sub>	0.41	0.43	0.42	0.49	0.46	0.45
Al <sub>2</sub> O <sub>3</sub>	17.33	17.50	17.60	17.04	18.11	18.19
Fe <sub>2</sub> O <sub>3</sub> tot	3.10	3.09	3.06	3.44	3.38	3.51
MnO	0.20	0.19	0.20	0.14	0.15	0.14
MgO	0.23	0.24	0.21	0.42	0.45	0.50
CaO	1.72	1.70	1.63	2.26	2.14	2.27
Na <sub>2</sub> O	6.02	5.81	5.98	4.18	4.91	4.79
K <sub>2</sub> O	6.68	6.90	6.65	7.58	7.98	8.43
P <sub>2</sub> O <sub>5</sub>	0.04	0.04	0.04	0.09	0.08	0.10
L.O.I.	3.74	3.31	3.87	3.64	2.88	2.80
Total	99.90	99.10	99.93	99.07	99.89	100.30
S	<0.01	0.01	0.02	nd	0.04	0.02
Cl	0.81	0.70	0.71	nd	0.67	0.72
F	0.30	0.25	0.28	nd	0.16	0.17
Be (ppm)	26	23	26	13	14	13
V	10	16	10	48	39	48
Zn	110	90	100	60	90	80
Ga	27	25	27	19	22	20
Ge	1.8	1.7	1.9	1.4	1.5	1.4
As	72	53	69	56	44	34
Rb	530	468	517	320	405	379
Sr	12	19	11	211	140	220
Y	78.0	66.0	75.6	33.8	43.2	38.0
Zr	1,096	982	1,118	477	558	501
Nb	131.0	111.0	132.0	59.6	69.4	61.8
Cs	60.4	51.0	59.9	26.0	35.1	31.3
Ba	5	<3	<3	110	52	108
La	180.0	152.0	178.0	97.4	103.0	92.4
Ce	326	281	326	170	191	170
Pr	35.0	30.2	34.9	16.9	20.5	18.2
Nd	115.0	100.0	114.0	55.2	70.1	61.5
Sm	19.1	17.0	19.4	10.7	12.3	10.7
Eu	1.5	1.4	1.3	1.8	2.0	2.0
Gd	14.6	12.8	14.5	8.1	9.5	8.3
Tb	2.4	2.1	2.3	1.1	1.5	1.3
Dy	13.0	11.1	12.7	6.1	7.8	6.7
Ho	2.5	2.1	2.4	1.2	1.5	1.3
Er	7.5	6.3	7.5	3.7	4.2	3.8
Tm	1.2	1.0	1.2	0.6	0.6	0.6
Yb	7.8	6.6	7.7	3.6	4.2	3.8
Lu	1.2	1.0	1.2	0.5	0.6	0.6
Hf	22.5	18.9	22.6	10.3	11.6	10.3
Ta	8.2	7.0	8.2	3.9	4.5	3.9
W	8.5	8.4	8.4	8.3	7.8	9.1
Pb	87	67	80	27	80	68
Th	94.9	77.9	94.4	41.7	48.1	42.8

**Table 1** continued

Member	A	A	A	A	Bt	Cmb
Sample	A0	A2b	A2t	A2t	Bt	Cmb
Location	1-Torreta	2-Amm.	2-Amm.	2-Amm.	3-Mte Russo	4-La Schiana
U	32.4	26.7	31.9	14.9	16.5	14.6
Ne	4.3	4.7	4.1	4.2	5.3	7.0
D.I.	91	90	90	90	87	87
A.I.	0.98	0.97	0.96	0.97	0.91	0.93

Differentiation Index, D.I.: normative (Or + Ab + Ne); CIPW norms are calculated assuming FeO/Fe<sub>2</sub>O<sub>3</sub> = 0.5 (Armienti et al. 1983)

Alkalic index, A.I. = [(Na<sub>2</sub>O + K<sub>2</sub>O)/Al<sub>2</sub>O<sub>3</sub>] molar ratio

L.O.I. loss on ignition, *nd* not determined, *Ne* normative nepheline

alkali trachyte end member (A0). Intermediate compositions are ascribed here to very small-scale syn-eruptive mingling (<10 µm, the analytical spot/window size) or mixing, as modeled by Perugini et al. (2010). Lastly, the Bt pumices and their matrices are essentially comparable to the less evolved trachyte (Member C), although a micro-scale heterogeneity was observed (Electronic appendix 2). We therefore conclude that two distinct magma batches were present before the Averno 2 eruption; these were intensively mingled in the course of the eruption, with an increasing proportion of the less evolved trachyte from the A2t to Bt fallout deposits.

All the matrices of the vesicular pumice are significantly degassed with respect to sulfur (S < 0.02 wt%; Fig. 6d). Water was not analyzed. Their F content varies from 0.23 to 0.46 wt%, whereas Cl averages at  $0.89 \pm 0.04$  wt% (Fig. 6e). With the exception of the Campanian Ignimbrite (Signorelli et al. 1999, 2001), there is little F data available for Phlegraean Field trachytes. The Cmb trachytic matrices plot on the F–Cl trend delineated by Cl trachytes (Fig. 6e), and the divergent behavior of Cl and F is fully in agreement with the higher solubility of F in hydrous silicic melts with respect to Cl (e.g., Carroll and Webster 1994). During crystal fractionation of highly evolved trachytic melts, F and Cl behave as incompatible elements but only Cl reaches its solubility limit (Signorelli et al. 2001) and is strongly partitioned into the H<sub>2</sub>O-rich vapor phase (e.g., Webster et al. 2009).

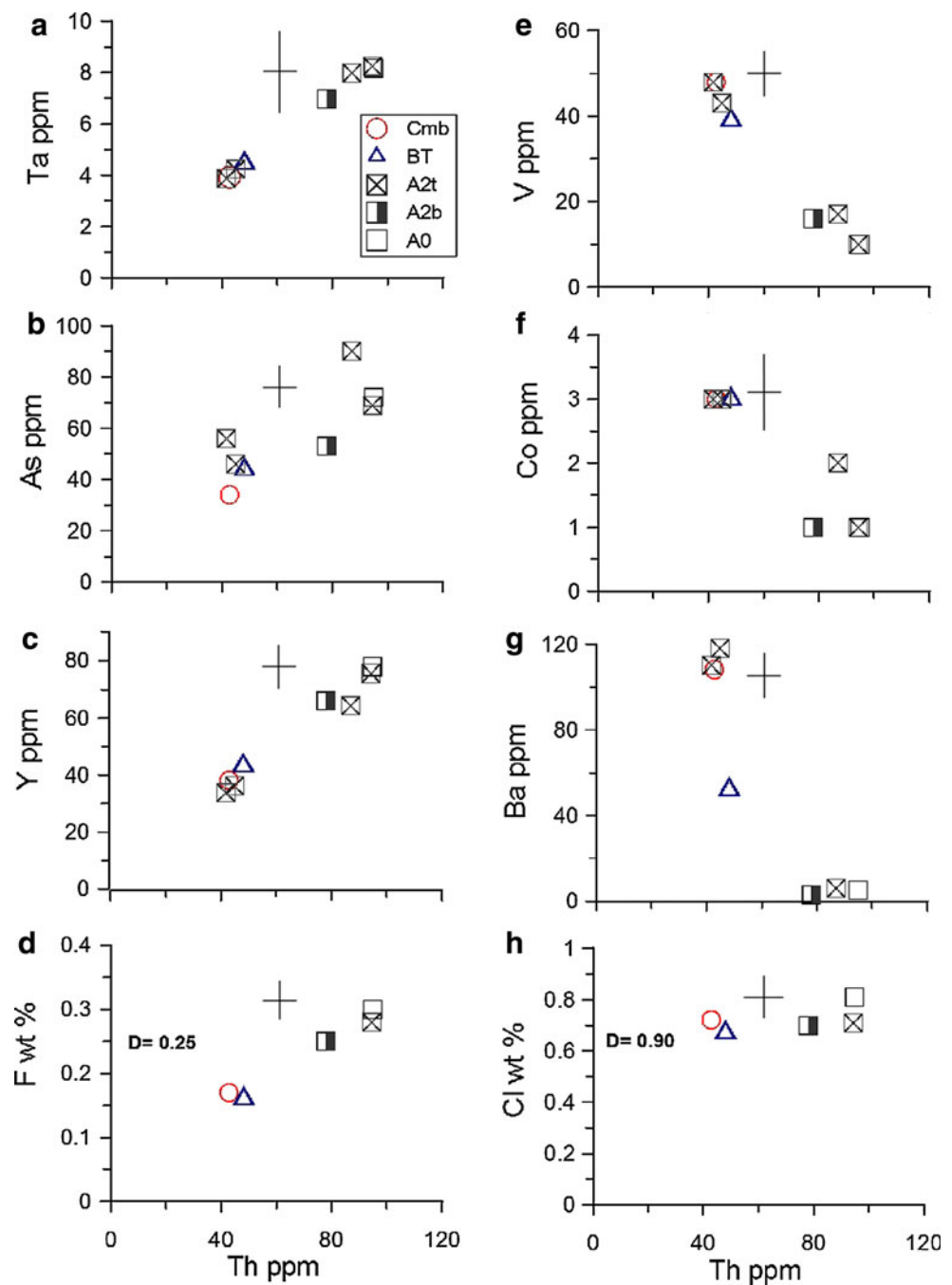
Melt inclusions trapped in clinopyroxene were analyzed in each fallout sample from the three tephra units (A–C). Several melt inclusions are present in both the homogenous and in the zoned crystals. They have faceted shapes, with a maximum size of 70 µm (Fig. 7a), as commonly observed in pumice from the Phlegraean Fields (e.g., Métrich 1983; Signorelli et al. 1999). The melt inclusions consist of brown glass, with one shrinkage bubble, and may contain apatite needles. Some isolated melt inclusions also occur at the diopside Fs<sub>5–10</sub>–Fs<sub>13–14</sub> interface of crystals showing oscillatory zoning (Fig. 7b).

The major- and volatile element composition of clinopyroxene-hosted melt inclusions is reported in Table 2 and

in the auxiliary materials; their evolution is depicted in Fig. 6b–f. Fluorine (0.20–0.61 wt%) is here considered to be a good tracer of melt differentiation due to its low bulk repartition coefficient, as shown above. As F increases, K<sub>2</sub>O concentrations decrease steadily, in accordance with the crystallization of K-feldspar (Fig. 6b). Na<sub>2</sub>O increases up to 6 wt% (F = 0.43 wt%) and then decreases to 5 wt%, a feature in agreement with plagioclase fractionation. The lowering of P<sub>2</sub>O<sub>5</sub> (from 0.16 to <0.04 wt%) recorded in melt inclusions is ascribed to the crystallization of apatite (Fig. 6c). Taken as a whole, the compositional range of melt inclusions is wider than that of the glassy matrices and the bulk rocks (Fig. 6a, b). The most evolved ones have much higher F contents (up to 0.61 wt%) and are found in the Fe richer clinopyroxene (Fs<sub>20–25</sub>) of samples A0 and A2b (Fig. 6c). Interestingly, they are even more evolved than the glassy matrices (Fig. 6b). The least evolved trachytic terms (F ≤ 0.25 wt%) are commonly found either at the interface between Mg- and Fe-rich diopside (Fs<sub>5–10</sub>–Fs<sub>13–14</sub>) or in Mg–Fe diopside (Fs<sub>12–16</sub>) in Cmb pumice (Fig. 6c). Most melt inclusions in samples A2b and A2t have a similar composition to that of melt inclusions in Cmb clinopyroxenes, testifying to the mechanical entrainment of crystals by the ascending magma.

Melt inclusions display variable total volatile contents (H<sub>2</sub>O + Cl + F + S) ranging from <3.0 up to 6.5 wt%. Carbon (CO<sub>2</sub> or carbonates) was not detected in melt inclusions (CO<sub>2</sub> ≤ 40 ppm). The H<sub>2</sub>O content of melt inclusions ranges between 0.4 and 5.0 wt%. The highest contents were observed in the most evolved MI (F ≥ 0.5 wt%) in sample A2b (Fig. 6f). However, inclusions in samples A0 and A2b (with similar degrees of evolution) may have lower H<sub>2</sub>O concentrations ( $3.3 \pm 0.08$  wt%, Fig. 6f). The least evolved inclusions (F ≤ 0.25 wt%) from samples Cmb and A2t display a decreasing abundance of H<sub>2</sub>O (from 3.1 to 1.3 wt%), whereas those from sample Bt are totally depleted in H<sub>2</sub>O (0.8–0.4 wt%). The lowest values most likely indicate that the melt inclusions were opened. Sulfur is strongly degassed (Fig. 6d), with the highest and lowest S

**Fig. 3** Variation diagrams of selected trace elements versus Th for Averno 2 whole rocks



concentrations (0.05 and 0.02 wt%) measured, respectively, in the least and most evolved melt inclusions from Cmb and A0 pumices. The Cl concentrations remain constant, as observed in the matrices, with an average concentration of  $0.90 \pm 0.02$  wt%; only a few inclusions in sample A0 show a slight increase in Cl to 1.0 wt% (Fig. 6e). As presented above, the effect of apatite crystallization on the behavior of halogens is marginal, whereas the behavior of Cl during magma evolution is most likely controlled by the effect of pressure-related Cl solubility and/or its partitioning between fluid and melt.

## Discussion

### The dominant process: crystal fractionation

The comparison between Averno 2 pumices and the PFc trachytic products erupted over the last 39 ky raises some interesting questions. Averno samples are among the most evolved PFc products, as they are more evolved than the NYT trachytes and even than the evolved CI alkali trachytes (Fig. 8a). The Averno alkali trachytes belong to the magma series emplaced during the last period of high



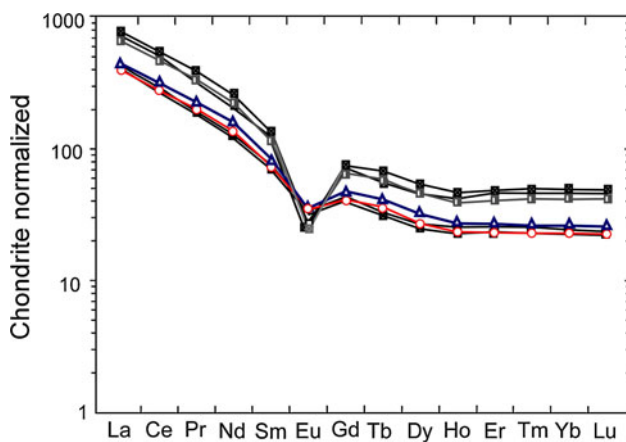


**Fig. 4** Chondrite-normalized REE abundance patterns for Averno 2 pumices. Normalization values are from Mc Donough and Sun (1995). Symbols as in Fig. 4

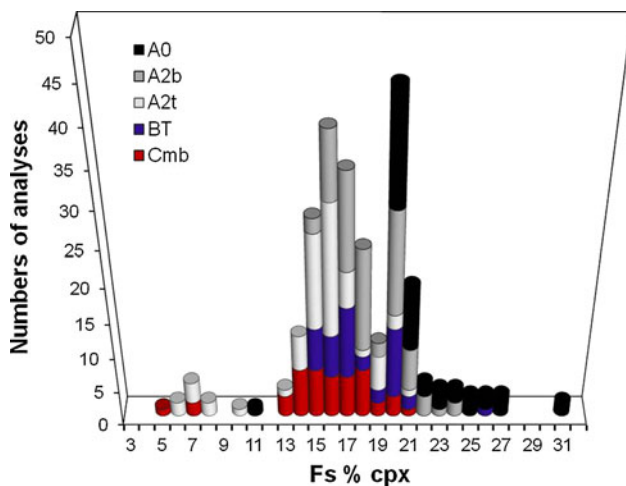


**Fig. 5** Histograms showing the distribution of clinopyroxene compositions in Members A (samples A0, A2b, and A2t), B (sample Bt), and C (sample Cmb)

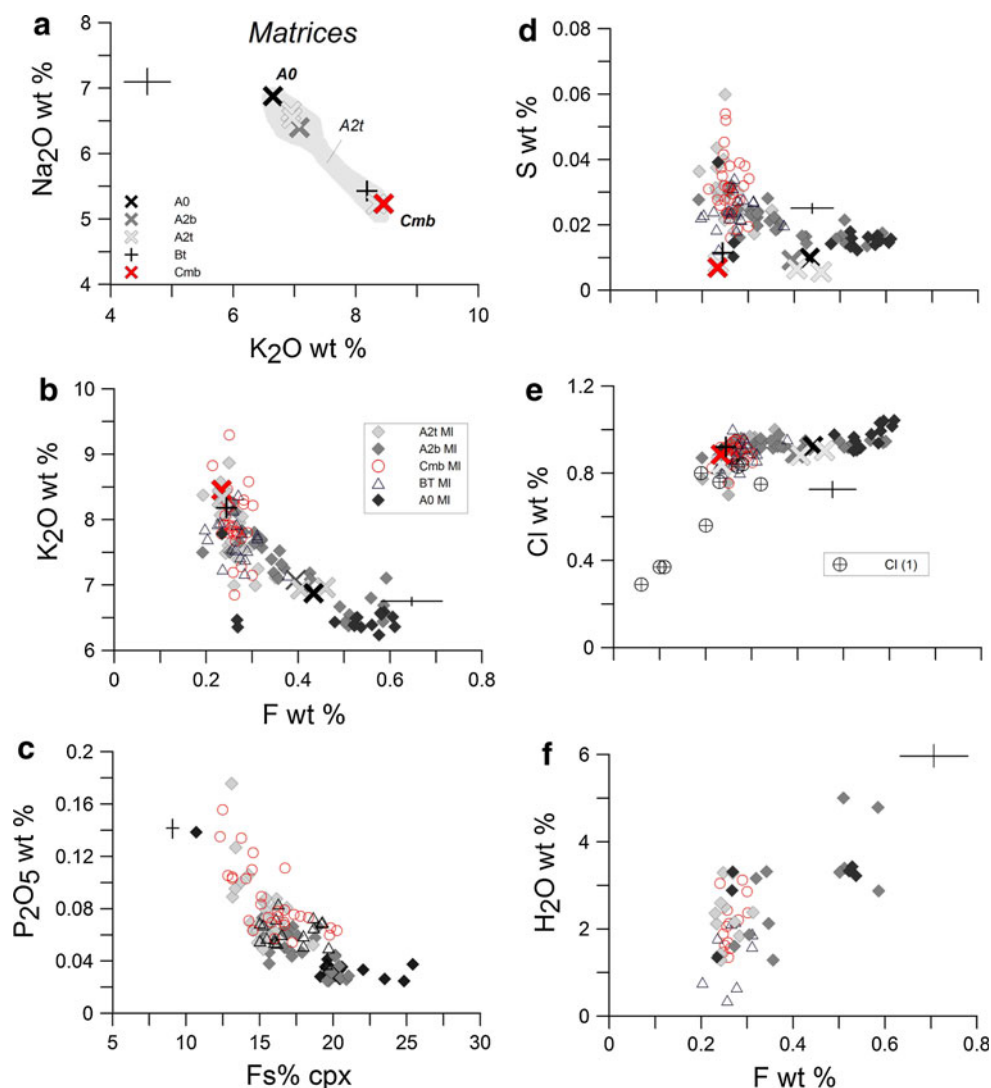
PfC activity dated between 4.8 and 3.8 ka (Orsi et al. 2004), filling the compositional gap between Astroni, AMS, and Monte Nuovo (Fig. 8a, b). They all display nearly constant Nb/Th (1.4) and Nb/Zr (0.15) ratios (Table 1), as measured in Minopoli 1 shoshonites erupted at 11.1 ka (Di Vito et al. 1999; Cannatelli et al. 2007). Such features strongly suggest that the trachytes were prevalently generated by crystal differentiation from a common parental magma. A process of crystal fractionation is supported by the chemical evolution of both Averno 2 pumices and melt inclusions (Figs. 3 and 6). From the base (samples A0 and A2b) to the top (sample Cmb), the alkali trachytes have parallel trace element patterns but an increasing negative Eu anomaly that is accounted for by

sanidine fractionation (Fig. 4). In order to illustrate the evolution path of the Averno melt, we used the “ANAMORPHOSIS” program, a method for projecting geochemical data by tracing the compositional variability of a sample set within a tetrahedron; details of the method are given by Armienti and Gasperini (2007). We assign here the four end members Albite (Ab), Anorthite (An), Orthoclase (Or), and Diopside (D) to the different vertices of the tetrahedron. For each member (A, B, and C) of the Averno 2 sequence, we projected the major element data on melt inclusions and glassy matrices, along with those of the coexisting feldspars, onto the anorthite-albite-orthoclase plane (Fig. 9). For each sample set, the melt compositions move along the plagioclase-alkali-feldspar cotectic curve (BC). However, the common rimming of plagioclase by alkali feldspar (anti-rapakivi texture) observed in the Averno samples indicates that plagioclase reached the “critical composition” corresponding to the termination of the plagioclase-alkali-feldspar surface (Armienti et al. 1983). Beyond this point, the boundary between the stability fields of plagioclase and alkali feldspar is a reaction curve (peritectic) along which plagioclase reacts with the liquid to produce alkali feldspar. The anti-rapakivi texture found in the Cmb sample indicates that crystals were transported mechanically. The K-feldspar clusters probably formed on the walls of the magma chamber and were subsequently entrained during the magma’s ascent to the surface.

The overall variation of Th in Averno bulk pumices (from 42.8 to 94.9 ppm) and the constant ratios between highly incompatible elements allow us to assess the extent of differentiation using Rayleigh’s distillation law  $C_i = C_0 f^{(D-1)}$ . Considering that Th has a very low bulk partition coefficient (Villemant 1988), the A0 and A2b pumices could have derived from the Cmb trachyte through ~55 wt% removal of solids, with feldspar as the dominant phase. We also calculated the bulk distribution coefficients (D) for Sr and Ba, two elements highly fractionated by the K-feldspars. For Sr, the derived D values are 4.9 and 4.7 when using the Nb and Th as incompatible elements, respectively (Fig. 8c, d). These values are in agreement with the  $D_{Sr}$  (2–6.6) measured for feldspars in PFC trachytes (Villemant 1988).  $D_{Ba}$  is higher and equal to 5.5.

Some clinopyroxenes in Averno 2 samples show Mg-diopside zones or relict cores, as commonly described in the products of the Phlegraean Fields (e.g., Arienzo et al. 2009, 2010). Mg-rich diopside ( $Wo_{47.5}$ ,  $Fs_{6-8}$ ) from the trachybasaltic magma of the Minopoli 2 eruption in the Phlegraean Fields was found to crystallize at 1,150–1,160°C (Métrich 1983; Cannatelli et al. 2007). Their occurrence in Averno pumices is consistent with a

**Fig. 6** Variation diagrams for major and volatile elements in melt inclusions and glassy matrices of the Averno 2 sequence. **a** Evolution of Na<sub>2</sub>O and K<sub>2</sub>O in the glassy matrices analyzed by SEM. Systematic analysis of A2t and Bt glassy matrices revealed their heterogeneity at the micrometer scale. **b** K<sub>2</sub>O versus F plot showing that the composition of melt inclusions in A0 clinopyroxenes is systematically more evolved than that of the A0 glassy matrix. **c** Variation of P<sub>2</sub>O<sub>5</sub> in melt inclusions as a function of their host clinopyroxene composition expressed as Fs mol%. **d–f** Evolution of dissolved volatiles (S, Cl, and H<sub>2</sub>O) versus F in melt inclusions and glassy matrices. Cl concentrations in the matrices and melt inclusions of C.I. pumices are reported in Plot 6e for comparison (data from Signorelli et al. 2001) (see text for “Discussion”)



process of crystal fractionation from less evolved parental melts.

We therefore conclude that the evolution of Averno 2 trachytic magmas is accounted for by fractional crystallization. This does not exclude the contribution of mixing (Perugini et al. 2010) between melts belonging to the same differentiation series. This conclusion most likely holds for trachytic magmas erupted over the last 4,000 years in the Phlegraean Fields area.

Lastly, we found a direct relationship between the chemical composition of the erupted magmas and their volume, even taking into account that the error in volume estimation is much larger than that in the geochemical parameters (Biass and Bonadonna 2011). Note that the volumes of the most evolved trachytic magmas are the smallest, and this supports the hypothesis of a common source for all Phlegraean magmas and their differentiation by crystal fractionation (Fig. 8b).

#### Averno melt saturation pressures and ascent dynamics

The dominant volatile species in Averno melt inclusions is water. The absence of detectable dissolved molecular CO<sub>2</sub> and carbonate ions suggests that CO<sub>2</sub> was lost before low-pressure crystallization and melt entrapment. This feature was observed not only in Averno samples but also in CI (Signorelli et al. 1999, 2001; Marianelli et al. 2006) and AMS (Arienzo et al. 2010) trachytes.

Assuming that Averno trachytes mainly derived through fractional crystallization of a deep-settled trachybasaltic/shoshonitic magma containing 2.8 wt% H<sub>2</sub>O (Mangiacapra et al. 2008), their H<sub>2</sub>O content would largely exceed 5 wt%. Most Averno melt inclusions contain between 1.5 and 5 wt% H<sub>2</sub>O, instead, which is the range prevalently reported for PFC trachytes (Fig. 10). Actually, CO<sub>2</sub> fluxing could be a very efficient process to remove water from deep melts ( $\geq 10$  km) in the Phlegraean Fields plumbing

**Table 2** Selected compositions of melt inclusions and glassy matrices of the Averno 2 pumices

Sample inclusion	A0					A2b							A2t						
	MI-3b	MI-5	MI-3a	Matrix <sup>d</sup>		MI-3	MI-6	MI-7a	MI-9	MI-1	Matrix <sup>d</sup>		MI-13	MI-16	Matrix A <sup>d</sup>		Matrix B <sup>d</sup>		
	3,1	3,1	5,1	12,3	SD	3,1	3,1	2,1	5,1	3,1	12,3	SD	4,1	3,1	7,1	SD	5,1	SD	
N,n <sup>a</sup>	3,1	3,1	5,1	12,3	SD	3,1	3,1	2,1	5,1	3,1	12,3	SD	4,1	3,1	7,1	SD	5,1	SD	
SiO <sub>2</sub> <sup>b</sup>	60.28	59.52	60.96	61.39	(16)	60.78	58.94	59.94	59.04	58.07	61.14	(48)	59.76	59.97	60.16	(23)	61.68	(30)	
TiO <sub>2</sub>	0.37	0.37	0.47	0.40	(2)	0.49	0.48	0.37	0.45	0.42	0.45	(7)	0.41	0.51	0.43	(7)	0.35	(10)	
Al <sub>2</sub> O <sub>3</sub>	16.95	17.47	17.26	18.54	(9)	17.89	17.14	17.75	17.83	17.13	18.57	(12)	17.66	17.01	18.80	(17)	18.55	(38)	
FeO <sub>total</sub>	3.06	2.79	2.79	2.93	(3)	3.18	3.01	2.45	2.98	1.49	2.95	(5)	2.97	3.11	3.26	(13)	2.76	(25)	
MnO	0.25	0.18	0.25	0.26	(5)	0.24	0.26	0.15	0.17	0.18	0.25	(2)	0.18	0.19	0.17	(8)	0.25	(12)	
MgO	0.20	0.14	0.24	0.33	(4)	0.30	0.14	0.11	0.28	0.27	0.33	(4)	0.33	0.25	0.48	(4)	0.35	(5)	
CaO	1.73	1.34	1.66	1.78	(5)	1.90	1.45	1.23	1.82	2.83	1.96	(16)	1.84	1.73	2.32	(7)	1.73	(9)	
Na <sub>2</sub> O	5.49	5.77	4.75	6.65	(2)	5.65	5.68	5.98	5.24	5.75	6.40	(20)	4.65	4.99	5.23	(10)	6.54	(21)	
K <sub>2</sub> O	6.51	6.40	6.47	6.88	(3)	7.19	6.38	6.43	7.69	6.44	7.08	(21)	7.61	7.25	8.34	(5)	6.96	(24)	
P <sub>2</sub> O <sub>5</sub>	0.03	0.03	0.01	0.03	(1)	0.06	0.03	0.03	0.06	0.03	0.04	(9)	0.06	0.05	0.08	(9)	0.04	(8)	
S	0.013	0.018	0.026	0.010		0.021	0.022	0.017	0.022	0.015	0.009	(1)	0.022	0.017	0.008	(3)	0.006	(7)	
Cl	0.905	0.903	0.912	0.925	(79)	0.915	0.918	0.920	0.918	0.946	0.892	(23)	0.891	0.904	0.839	(75)	0.904	(45)	
F	0.528	0.522	0.268	0.434	(23)	0.347	0.509	0.501	0.319	0.584	0.395	(34)	0.248	0.313	0.235	(42)	0.459	(45)	
H <sub>2</sub> O	3.4	3.3	2.9	nd		2.1	5.0	3.4	3.2	4.8	nd		3.3	2.4	nd		nd		
Total	99.74	98.78	99.39	100.56		101.07	99.94	99.26	99.98	98.93	100.46		99.92	98.68	100.35		100.58		
<i>Host pyroxene</i>																			
SiO <sub>2</sub>	50.3	50.7	50.7			50.5	49.6	49.8	50.2	50.4			50.8	50.3					
TiO <sub>2</sub>	0.5	0.5	0.8			1.0	0.7	0.6	0.6	0.5			0.7	0.7					
Al <sub>2</sub> O <sub>3</sub>	1.3	3.1	2.6			3.0	2.2	1.9	2.3	1.8			2.4	1.9					
FeO	14.1	11.2	11.7			11.3	12.4	11.9	9.5	11.8			9.5	10.9					
MnO	1.4	1.1	0.8			0.9	0.9	1.0	0.7	0.9			0.6	1.0					
MgO	8.1	9.7	9.4			11.4	10.3	10.1	11.9	10.7			11.6	10.6					
CaO	22.1	21.2	22.4			22.3	22.4	22.8	23.5	22.7			22.9	22.4					
Na <sub>2</sub> O	0.6	0.9	0.6			0.7	0.8	0.6	0.5	0.6			0.5	0.6					
Total	98.5	98.8	99.0			101.0	99.4	98.8	99.1	99.4			99.1	98.3					
Wo <sup>c</sup>	49.7	48.9	50.3			47.5	48.3	49.4	49.6	48.6			49.2	49.1					
En	25.4	31.0	29.2			33.8	30.8	30.4	34.8	31.7			34.8	32.3					
Fs	24.8	20.1	20.5			18.8	20.9	20.1	15.6	19.7			16.0	18.6					
Mg <sup>#c</sup>	50.6	60.7	58.8			64.3	59.6	60.2	69.0	61.7			68.5	63.4					

**Table 2** continued

Sample	Bt				Cmb						
	MI-6	MI-7	Matrix <sup>d</sup>		MI-1	MI-3	MI-28	Matrix <sup>d</sup>		Obsidian clasts	
N,n <sup>a</sup>	3,1	2,1	9,2	SD	3,1	3,1	3,1	9,2	SD	33,4	SD
SiO <sub>2</sub> <sup>b</sup>	59.91	60.64	60.28	(2)	58.66	59.02	60.85	59.94	(4)	59.48	(40)
TiO <sub>2</sub>	0.41	0.44	0.42	(6)	0.37	0.46	0.54	0.44	(1)	0.43	(3)
Al <sub>2</sub> O <sub>3</sub>	17.96	17.97	18.87	(23)	18.57	17.11	17.77	18.86	(3)	18.11	(9)
FeO <sub>total</sub>	3.25	3.37	3.10	(1)	3.07	3.39	3.34	3.25		3.14	(11)
MnO	0.18	0.11	0.17	(4)	0.03	0.20	0.21	0.21	(3)	0.15	(5)
MgO	0.35	0.35	0.46	(1)	0.57	0.35	0.36	0.50	(3)	0.41	(4)
CaO	1.90	1.92	2.23		2.15	2.11	2.09	2.27	(3)	2.03	(11)
Na <sub>2</sub> O	4.72	4.80	5.41	(5)	4.41	4.35	5.40	5.23	(0)	5.02	(13)
K <sub>2</sub> O	7.72	7.43	8.20	(1)	8.22	8.07	7.15	8.46	(4)	7.71	(16)
P <sub>2</sub> O <sub>5</sub>	0.07	0.05	0.07	(1)	0.13	0.09	0.05	0.08	(3)	0.08	(1)
S	0.027	0.018	0.012		0.034	0.038	0.020	0.007	(1)	0.011	(4)
Cl	0.891	0.804	0.920	(23)	0.850	0.910	0.892	0.886	(42)	0.898	(26)
F	0.311	0.274	0.244	(6)	0.301	0.241	0.300	0.233	(20)	0.285	(27)
H <sub>2</sub> O	1.9	2.2	nd		2.4	3.0	2.9	nd		1.3	(2)
Total	99.60	100.36	100.38		99.75	99.37	101.83	100.37		99.07	
<i>Host pyroxene</i>											
SiO <sub>2</sub>	50.5	51.5			50.2	50.9	50.3				
TiO <sub>2</sub>	0.6	0.5			0.7	0.6	0.9				
Al <sub>2</sub> O <sub>3</sub>	2.9	2.1			3.4	2.8	2.8				
FeO	9.0	9.7			8.3	8.9	10.2				
MnO	0.6	0.6			0.4	0.4	0.7				
MgO	12.2	11.7			12.9	12.0	11.3				
CaO	22.6	23.0			22.5	22.6	22.4				
Na <sub>2</sub> O	0.5	0.5			0.5	0.5	0.6				
Total	99.0	99.6			98.8	98.7	99.2				
Wo <sup>c</sup>	48.5	49.0			48.0	48.8	48.7				
En	36.5	34.8			38.3	36.1	34.1				
Fs	15.0	16.2			13.8	15.1	17.2				
Mg# <sup>c</sup>	70.8	68.2			73.6	70.5	66.5				

SD standard deviation, MI melt inclusions, nd not determined

<sup>a</sup> N,n: Average of N analyses in n melt inclusions or in glassy matrices<sup>b</sup> Oxides and element analyses given in wt%<sup>c</sup> Wollastonite, Enstatite, Ferrosilite components; Mg#: 100xMg/(Mg + Fe<sup>2+</sup>)<sup>d</sup> Major and minor elements analyzed by SEM and Electron microprobe, respectively (see text and electronic appendix 2)



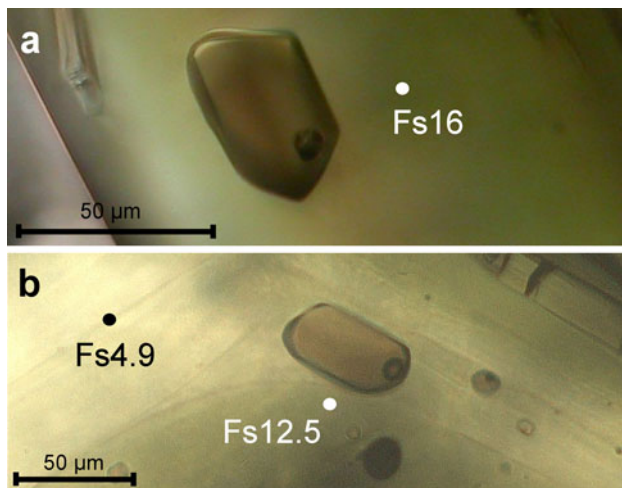


**Fig. 7** Transmitted light photomicrographs of typical melt inclusions in the pyroxene of Averno 2 magma. **a** melt inclusion with typical faceted shape. **b** isolated melt inclusion at the Mg–Fe-rich diopside interface

system, as previously suggested by Mangiacapra et al. (2008), a process not recorded in Averno samples.

A trachytic melt containing 5 wt%  $H_2O$  but negligible amounts of  $CO_2$  achieves saturation at a total fluid pressure ( $P_{TOT} = P_{H_2O}$ ) of 100 MPa according to experimental solubility data available for trachytic melts at 875°C (Di Matteo et al. 2004). This  $P_{H_2O}$  value would correspond to the emplacement of a trachytic magma batch (A2b

samples) at a lithostatic depth of 4.4 km for a host-rock density of  $\sim 2,300 \text{ kg m}^{-3}$  (Rosi and Sbrana 1987). Such a high  $H_2O$  content was measured in two melt inclusions only (Figs. 6f and 10). Alternatively, an average  $H_2O$  content of  $\sim 3 \text{ wt\%}$  and F content ranging from 0.25 to 0.5 wt% (Fig. 6f) may indicate magma saturation with respect to a  $H_2O$ -rich vapor phase, for a total pressure ( $P_{H_2O}$ ) of 50 MPa. Magmas would be water-saturated and thus stored and/or emplaced at a depth of  $\sim 2 \text{ km}$ , as often reported in the Phlegraean Fields (e.g., Signorelli et al. 2001; Arienzo et al. 2009).

A vertically extended magma reservoir, with the top level saturated in a  $H_2O$ -rich vapor phase at a depth of 2–4 km is inconsistent with the geochemistry of Averno 2 magma and with the coexistence of magma batches with differing degrees of differentiation. We thus conclude that two distinct magma pockets stored at a depth of 2–4 km and evolving independently, with no direct connection with the deepest portions of the PFC reservoir, were successively involved in the Averno 2 eruption. This interpretation is sustained by (1) the conclusions drawn by Di Vito et al. (2010), who identified two magma batches with distinct  $^{87}\text{Sr}/^{86}\text{Sr}$  ratios (0.707507 and 0.707531), and by (2) the syn-eruptive mingling between two distinct magma batches, as illustrated by the coexistence of pumice clasts of different composition in the intermediate fallout layers of the Averno 2 sequence. In the Phlegraean Fields area, magma mingling is commonly invoked to explain the

**Fig. 8** Variation diagrams of **a** La versus Ce, **b** Nb versus Zr, **c**  $\log(\text{Sr})$  versus  $\log(\text{Nb})$ , and **d**  $\log(\text{Sr})$  versus  $\log(\text{Th})$ . The Sr repartition coefficient between mineral and melt ( $D_{Sr}$ ) was deduced from the slopes ( $1-D_i$ ) of linear trends in log–log plots. For comparison, we have plotted the available data on the Phlegraean Fields from the literature: (1) Campanian Ignimbrite (CI) from Civetta et al. (1997), Arienzo et al. (2009); (2) Neapolitan Yellow Tuff (NYT) from Orsi et al. (1995); (3) Minopoli and Fondo Riccio from Villemant (1988), Beccaluva et al. (1991), Cannatelli et al. (2007); (4) Agnano Monte Spina (AMS) from De Vita et al. (1999); (5) Astroni from Tonnarini et al. (2009); and (6) Monte Nuovo (MN) from D’Orlando et al. (2005) and (7) Averno 2 from Di Vito et al. (2010)

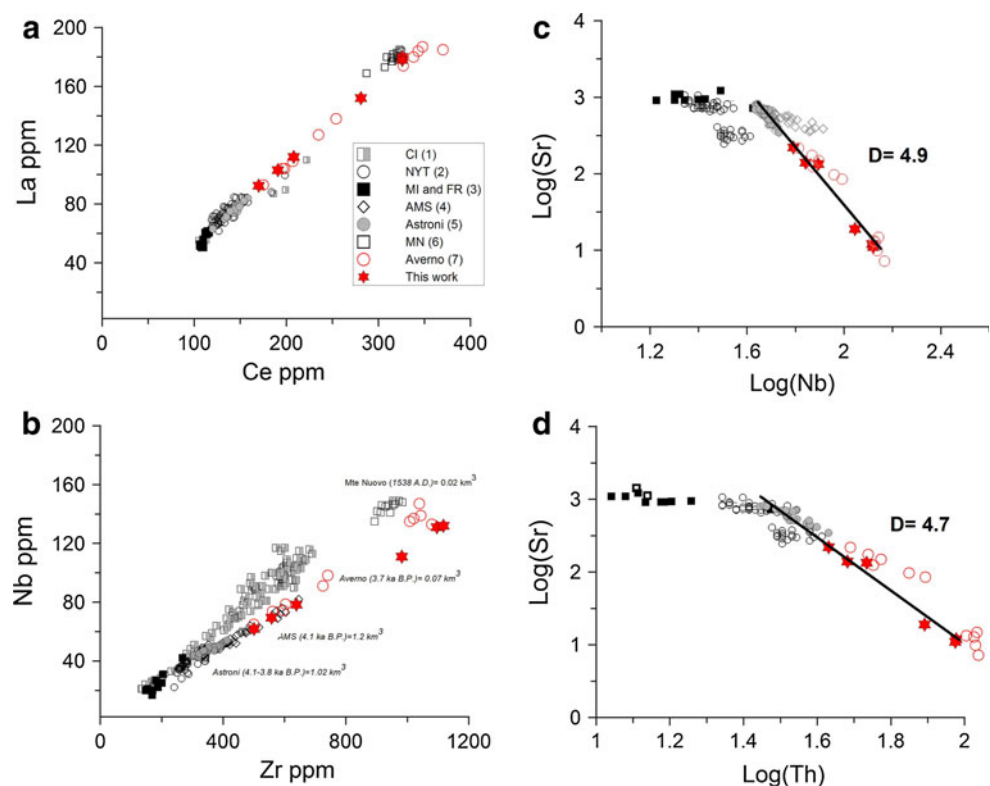


**Fig. 9** Projection of Averno 2 melt and feldspar compositions onto the Ab-An-Or plane

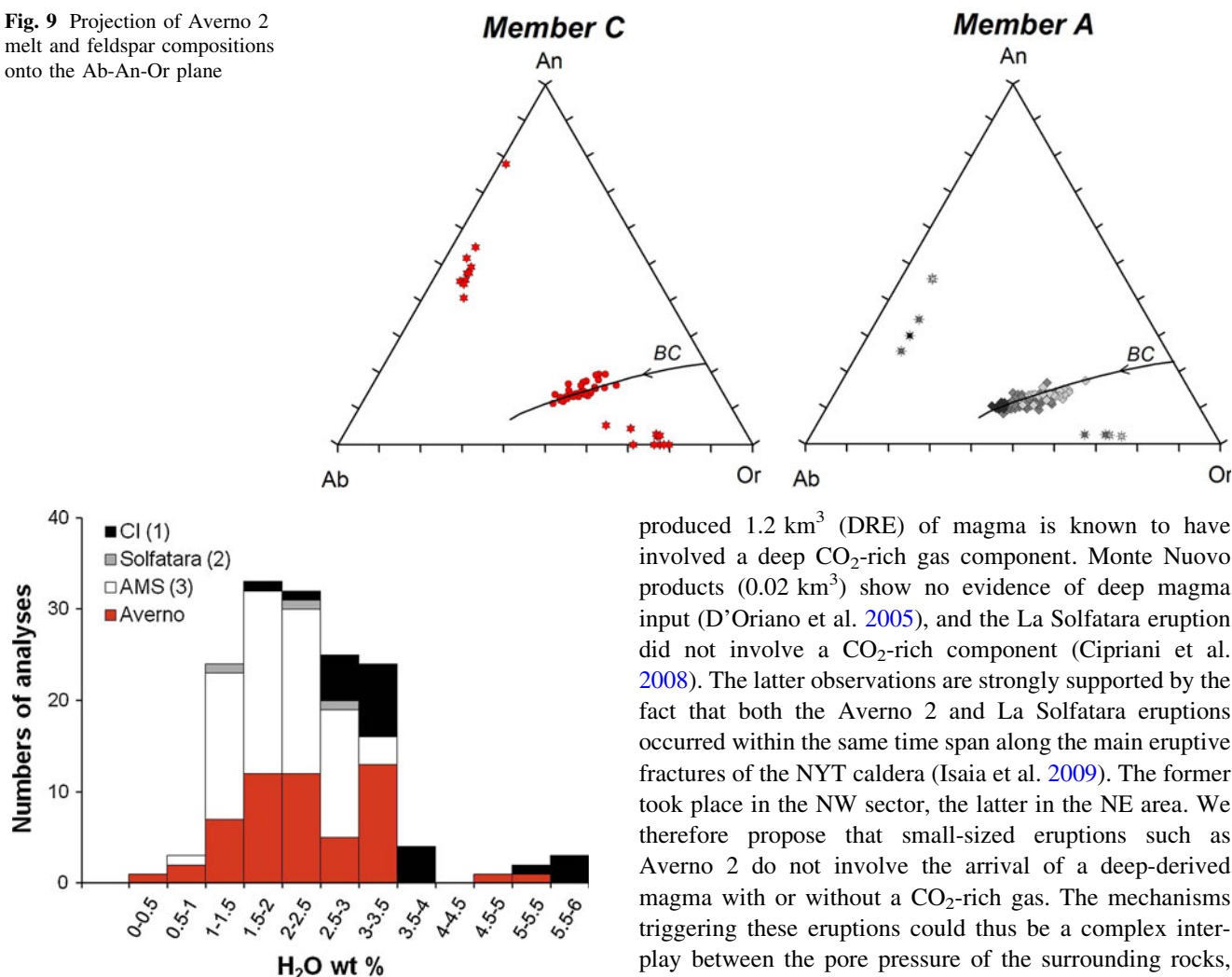


**Fig. 10** Distribution histogram of H<sub>2</sub>O contents in Averno 2 trachytic melt inclusions. We also report available data from the literature: (1) Campanian Ignimbrite (CI) from Signorelli et al. (2001), Marianelli et al. (2006), (2) Solfatara from Cipriani et al. (2008), and (3) Agnano Monte Spina (AMS) from Arienzo et al. (2010)

coexistence of melts differing either in their degree of evolution or their Sr–Nd isotopic ratios (e.g., Orsi et al. 1995; Civetta et al. 1997; Di Vito et al. 1999; Tonarini et al. 2004, 2009; Arienzo et al. 2009). However, note that during the Averno 2 event, magma mingling corresponded to the climactic phase of the eruption and to the maximum magma discharge rate. These features are consistent with a new magma influx or the withdrawal of independent magma ponding zones.

In the case of Averno 2 samples, the absence of melt inclusions with a less differentiated composition (shoshonite), such as those found in Minopoli 2 (Mangiacapra et al. 2008), suggests that a deep-derived magma was not involved in the eruption. This is a particularly interesting point because in the last 5 ka, only the AMS eruption that

produced 1.2 km<sup>3</sup> (DRE) of magma is known to have involved a deep CO<sub>2</sub>-rich gas component. Monte Nuovo products (0.02 km<sup>3</sup>) show no evidence of deep magma input (D’Orlando et al. 2005), and the La Solfatara eruption did not involve a CO<sub>2</sub>-rich component (Cipriani et al. 2008). The latter observations are strongly supported by the fact that both the Averno 2 and La Solfatara eruptions occurred within the same time span along the main eruptive fractures of the NYT caldera (Isaia et al. 2009). We therefore propose that small-sized eruptions such as Averno 2 do not involve the arrival of a deep-derived magma with or without a CO<sub>2</sub>-rich gas. The mechanisms triggering these eruptions could thus be a complex interplay between the pore pressure of the surrounding rocks, the rupture threshold, and possibly the flux of heat and gas preceding the ascent of the magma batch.

Lastly, we note the divergent behavior of Cl and F in Averno trachytic magmas, in agreement with the higher solubility of F with respect to Cl in hydrous silicic melts (e.g., Carroll and Webster 1994). The experimentally determined solubility of chlorine in hydrous trachytes at 860–930°C indicates that the amount of Cl dissolved in the melt decreases from 0.90 to 0.37 wt% as the pressure increases from 25 to 250 MPa (Signorelli and Carroll 2002). Based on these solubility experiments, the Averno trachytic melts, containing on average 0.90 wt% Cl, would have been saturated at 25 MPa (Signorelli et al. 2001), a pressure lower than that deduced from the H<sub>2</sub>O data. This finding suggests that Cl is mainly controlled by its partitioning in the H<sub>2</sub>O-rich vapor phase prior to eruption rather than the saturation pressure. This hypothesis is supported by the similarity between the Cl contents measured in melt inclusions and glassy matrices. Using the proportion of each of the volatile species in the least and more evolved trachytic melt inclusions, respectively, we assessed that the

gas phase released at the onset of the eruption would have been hydrosaline, with 0.81 mol % H<sub>2</sub>O and 0.18 mol % Cl.

## Conclusions

Detailed mineralogy and melt inclusion studies on pumice fallouts accurately positioned in the stratigraphic column have provided a framework for the interpretation of the sub-Plinian eruption that built the Averno 2 tuff ring 3.7 ka ago. Averno magma differentiation was prevalently controlled by a process of crystal fractionation. Emitted products fill the composition gap between trachytes erupted 5 ka ago and the youngest trachy-phonolites of the neighboring Monte Nuovo cone. Even though the volumes of the most evolved trachytic magmas are the smallest, the total volume of products emitted during an eruption is not directly correlated with their degree of differentiation. The chemical heterogeneity recorded in the Averno 2 sequence testifies to the coexistence of trachytic magma batches with different degrees of crystallization that mingled at the time of eruption. The successive extraction of magma batches independent of one another occurred when the magma discharge rate was greatest.

We suggest that the Averno 2 eruption resulted from the successive ascent of two small-volume magma pockets emplaced at shallow depth (2–4 km), without a significant contribution from deep-seated magmas. These results have important implications for hazard assessment in the area, because magma batches of similar size cannot be detected by classical geophysical methods.

**Acknowledgments** We are grateful to G. Orsi and M. Di Vito for their help in sampling the Averno 2 sequence, to L. Civetta for the stimulating discussions in the early stages of this work, to P. Fulignati and P. Marianelli for providing the statistics on SEM–EDS standard data, and to P. Armienti for providing the Anamorphosis program and helpful discussion. G. Moore and an anonymous reviewer are thanked for their suggestions and critical comments that significantly improved the manuscript. Financial support was provided by Dipartimento di Scienze della Terra, Speed Project “Scenari di pericolosità per la prevenzione del rischio dei vulcani della Campania” and IPGP contribution 3259.

## References

- Alessio M, Bella F, Improta S, Belluomini G, Cortesi C, Turi B (1971) University of Rome carbon-14 dates IX. *Radiocarbon* 13(2):395–411
- Allard P, Maiorani A, Tedesco D, Cortecchi G, Turi B (1991) Isotopic study of the origin of sulfur and carbon in Solfatara fumaroles, Campi Flegrei caldera. *J Volcanol Geotherm Res* 48:39–159
- Amoruso A, Crescentini L, Berrino G (2008) Simultaneous inversion of deformation and gravity changes in a horizontally layered half-space: evidences for magma intrusion during the 1982–1984 unrest at Campi Flegrei caldera (Italy). *Earth Planet Sci Lett* 272:181–188
- Arienzo I, Moretti R, Civetta L, Orsi G, Papale P (2010) The feeding system of Agnano-Monte Spina eruption (Campi Flegrei, Italy): dragging the past into present activity and future scenarios. *Chem Geol* 270:135–147
- Arienzo I, Civetta L, Heumann A, Wörner G, Orsi G (2009) Isotopic evidence for open system processes within the Campanian Ignimbrite (Campi Flegrei–Italy) magma chamber. *Bull Volcanol* 71:285–300
- Armienti P, Gasperini A (2007) Do we really need mantle components to define mantle composition? *J Petrol.* doi:10.1093/ptrology/egl078
- Armienti P, Barberi F, Bizouard H, Clocchiatti R, Innocenti F, Métrich N, Rosi M, Sbrana A (1983) The Phlegraean Fields: magma evolution within a shallow chamber. *J Volcanol Geotherm Res* 17:289–311
- Barberi F, Carapezza M, Innocenti F, Luongo G, Santacroce R (1989) The problem of volcanic unrest: the Phlegraean Fields case history. *Atti Convegni Lincei* 80:387–405
- Beccaluva L, Di Girolamo P, Serri G (1991) Petrogenesis and tectonic setting of the Roman volcanic Province (Italy). *Lithos* 26:191–221
- Biass S, Bonadonna C (2011) A quantitative uncertainty assessment of eruptive parameters derived from tephra deposits: the example of two large eruptions of Cotopaxi volcano, Ecuador. *Bull Volcanol.* doi:10.1007/s00445-010-0404-5
- Caliro S, Chiodini G, Moretti R, Avino R, Granieri D, Russo M, Fiebig J (2007) The origin of the fumaroles of La Solfatara (Campi Flegrei, South Italy). *Geochim Cosmochim Acta* 71:3040–3055
- Cannatelli C, Lima A, Bodnar RJ, De Vivo B, Webster JD, Fedele L (2007) Geochemistry of melt inclusions from the Fondo Riccio and Minopoli 1 eruptions at Campi Flegrei (Italy). *Chem Geol* 237:418–432
- Carroll MR, Webster JD (1994) Solubilities of sulfur, noble gases, nitrogen, chlorine, and fluorine in magmas. *Volatiles in magmas* (Carroll MR, Holloway JR Eds). *Mineral* 30:231–280
- Chiodini G, Frondini F (2001) Carbon dioxide degassing from the Albani Hills volcanic region, Central Italy. *Chem Geol* 177:67–83
- Chiodini G, Caliro S, Cardellini C, Granieri D, Avino R, Baldini A, Donnini M, Minopoli C (2010) Long-term variations of the Campi Flegrei, Italy, volcanic system as revealed by the monitoring of hydrothermal activity. *J Geophys Res* 115, B03205. doi:10.1029/2008JB006258
- Cipriani F, Marianelli P, Sbrana A (2008) Studio di una sequenza piroclastica del vulcano della Solfatara (Campi Flegrei). *Atti Società Toscana Scienze Naturali Memorie Serie A* 113:1–6
- Civetta L, Innocenti F, Sbrana A, Taddeucci G (1988) Variazioni petrografiche e geochimiche nei prodotti di Averno: implicazioni sulla zonatura del sistema di alimentazione. *Boll Gr Naz Vulcanol* IV:201–217
- Civetta L, Orsi G, Pappalardo L, Fisher RV, Heiken G, Ort M (1997) Geochemical zoning, mingling, eruptive dynamics and depositional processes, the Campanian Ignimbrite, Campi Flegrei Caldera, Italy. *J Volcanol Geoth Res* 75:183–219
- D’Antonio M, Civetta L, Orsi G, Pappalardo L, Piochi M, Carandente A, De Vita S, Di Vito MA, Isaia R (1999) The present state of the magmatic system of the Campi Flegrei caldera based on a reconstruction of its behaviour in the past 12 ka. *J Volcanol Geotherm Res* 91:247–268
- D’Orlando C, Poggianti E, Bertagnini A, Cioni R, Landi P, Polacci M, Rosi M (2005) Changes in eruptive style during the A.D. 1538 Monte Nuovo eruption (Phlegraean Fields, Italy): the role of syn-eruptive crystallization. *Bull Volcanol* 607:601–621

- De Natale GF, Troise C, Pingue F, Mastrolorenzo G, Pappalardo L, Battaglia M, Boschi E (2006) The Campi Flegrei caldera: unrest mechanisms hazards. *Geol Soc Lon Spec Publ* 269:25–45
- De Vita S, Orsi G, Civetta L, Carandente A, D'Antonio M, Deino A, Di Cesare T, Di Vito MA, Fisher RV, Isaia R, Marotta E, Necco A, Ort MH, Pappalardo L, Piochi M, Southon J (1999) The Agnano-Monte Spina eruption (4100 years B.P.) in the restless Campi Flegrei caldera. *J Volcanol Geotherm Res* 91:269–301
- De Vivo B, Rolandi G, Gans PB, Calvert A, Bohrsen WA, Spera FJ, Belkin HE (2001) New constraints on the pyroclastic eruptive history of the Campanian volcanic Plain (Italy). *Mineral Petrol* 73:47–65
- Deino AL, Orsi G, De Vita S, Piochi M (2004) The age of the Neapolitan Yellow Tuff caldera-forming eruption (Campi Flegrei caldera—Italy) assessed by  $^{40}\text{Ar}/^{39}\text{Ar}$  dating method. *J Volcanol Geotherm Res* 133:157–170
- Di Matteo V, Carroll MR, Beherens H, Vetere F, Brooker RA (2004) Water solubility in trachytic melts. *Chem Geol* 213:187–196
- Di Vito MA, Isaia R, Orsi G, Southon J, De Vita S, D'Antonio M, Pappalardo L, Piochi M (1999) Volcanism and deformation since 12,000 years at the Campi Flegrei caldera (Italy). *J Volcanol Geotherm Res* 91:221–246
- Di Vito MA, Arienzo I, Braia G, Civetta L, D'Antonio M, Di Renzo V, Orsi G (2010) The Averno 2 fissure eruption: a recent small-size explosive event at the Campi Flegrei Caldera (Italy) *Bull Volcanol*. doi:[10.1007/s00445-010-0417-0](https://doi.org/10.1007/s00445-010-0417-0)
- Ferrucci F, Hirn A, De Natale G, Virieux J, Mirabile L (1992) P-SV conversions at a shallow boundary beneath Campi Flegrei caldera (Italy): evidence for the magma chamber. *J Geophys Res* 97-NO.B11:15351–15359. doi:[10.1029/92JB00888](https://doi.org/10.1029/92JB00888)
- Fourmentaux C (2009) Eruptive processes in the Averno 2 eruption (Campi Flegrei, Italy): constraints by physical properties of the juvenile fragments and melt inclusions. PhD thesis, University of Pisa
- Isaia R, D'Antonio M, Dell'Erba F, Di Vito M, Orsi G (2004) The Astroni volcano: the only example of close eruptions within the same vent area in the recent history of the Campi Flegrei caldera (Italy). *J Volcanol Geotherm Res* 133:171–192
- Isaia R, Marianelli P, Sbrana S (2009) Caldera unrest prior to intense volcanism in Campi Flegrei (Italy) at 4.0 ka B.P.: implications for caldera dynamics and future eruptive scenarios. *Geophys Res Lett* 36. doi:[10.1029/2009GL040513](https://doi.org/10.1029/2009GL040513)
- Mangiaccapra A, Moretti R, Rutherford M, Civetta L, Orsi G, Papale P (2008) The deep magmatic system of the Campi Flegrei caldera (Italy). *Geophys Res Lett* 35:L21304
- Marianelli P, Sbrana A, Proto M (2006) Magma chamber of the Campi Flegrei supervolcano at the time of eruption of the Campanian Ignimbrite. *Geol* 34:937–940
- Mastrolorenzo G (1994) Averno Tuff ring in Campi Flegrei (south Italy). *Bull Volcanol* 56:561–572
- Mastrolorenzo G, Pappalardo L (2006) Magma degassing and crystallization processes during eruptions of high-risk Neapolitan-volcanoes: evidence of common equilibrium rising processes in alkaline magmas. *Earth Planet Sci Lett* 250:164–181
- Mc Donough WF, Sun S (1995) The composition of the Earth. *Chem Geol* 120:223–253
- Métrich N (1983) Les variations chimiques des clinopyroxènes calciques témoins de la complexité des processus pétrogénétiques à l'intérieur d'un réservoir magmatique. *Eur Bull Mineral* 106:353–364
- Métrich N, Clocchiatti R (1989) Melt inclusion investigation of the volatile behaviour in historic alkaline magmas of Etna. *Bull Volcanol* 51:185–198
- Mosbah M, Métrich N, Massiot P (1991) PIGME fluorine determination using a nuclear microprobe with application to glass inclusions: nuclear instruments and methods. *Phys Res B58*:227–231
- Orsi G, Civetta L, D'Antonio M, Di Girolamo P, Piochi M (1995) Step-filling and development of a three-layer magma chamber: the Neapolitan Yellow Tuff case history. *J Volcanol Geotherm Res* 67:291–312
- Orsi G, De Vita S, Di Vito M (1996) The restless, resurgent Campi Flegrei nested caldera (Italy): constraints on its evolution and configuration. *J Volcanol Geotherm Res* 74:179–214
- Orsi G, Civetta L, Del Gaudio C, De Vita S, Di Vito MA, Isaia R, Petrazzuoli SM, Ricciardi G, Ricco C (1999) Short-term ground deformations and seismicity in the resurgent Campi Flegrei caldera (Italy): an example of active block-resurgence in a densely populated area. *J Volcanol Geotherm Res* 91:415–451
- Orsi G, Di Vito MA, Isaia R (2004) Volcanic hazard assessment at the restless Campi Flegrei caldera. *Bull Volcanol* 66:514–530
- Pappalardo L, Civetta L, D'Antonio M, Deino AL, Di Vito MA, Orsi G, Carandente A, De Vita S, Isaia R, Piochi M (1999) Chemical and isotopic evolution of the Phlegraean magmatic system before the Campanian Ignimbrite 37 ka and the Neapolitan Yellow Tuff 12 ka eruptions. *J Volcanol Geotherm Res* 91:141–166
- Pappalardo L, Piochi M, D'Antonio M, Civetta L, Petrini R (2002) Evidence for multi-stage magmatic evolution during the past 60 Kyr at Campi Flegrei (Italy) Deduced from Sr, Nd and Pb isotope data. *J Petrol* 43:1415–1437
- Perugini D, Poli G, Petrelli M, De Campos CP, Dingwell DB (2010) Time-scales of recent Phlegraean fields eruptions inferred from the application of a 'diffusive fractionation' model of trace elements. *Bull Volcanol* 72(4):431–447
- Rosi M, Sbrana A (1987) The Phlegraean fields. *Quad Ric Sci CNR*, Rome, pp 1–175
- Signorelli S, Carroll MR (2002) Experimental study of Cl solubility in hydrous alkaline melts: constraints on the theoretical maximum amount of Cl in trachytic and phonolitic melts. *Contrib Mineral Petrol* 143:209–218
- Signorelli S, Vaggelli G, Francalanci L, Rosi M (1999) Origin of magmas feeding the Plinian phase of the Campanian Ignimbrite eruption, Phlegraean Fields, Italy: constraints based on matrix-glass and glass-inclusion compositions. *J Volcanol Geotherm Res* 91:199–220
- Signorelli S, Vaggelli G, Romano C, Carroll MR (2001) Volatile element zonation in Campanian Ignimbrite magmas (Phlegraean Fields, Italy): evidence from the study of glass inclusions and matrix glasses. *Contrib Mineral Petrol* 140:543–553
- Spilliaert N, Allard P, Métrich N, Sobolev AV (2006) Melt inclusion record of the conditions of ascent, degassing and extrusion of volatile-rich alkali basalt during the powerful 2002 flank eruption of Mount Etna (Italy). *J Geophys Res* 111:B04203
- Tonarini S, Leeman WP, Civetta L, D'Antonio M, Ferrara G, Necco A (2004) B/Nb and  $\delta^{11}\text{B}$  systematics in the phlegraean volcanic district (PVD). *J Volcanol Geotherm Res* 133:123–139
- Tonarini S, D'Antonio M, Di Vito MA, Orsi G, Carandente A (2009) Geochemical and B-Sr-Nd isotopic evidence for mingling and mixing processes in the magmatic system that fed the Astroni volcano (4.1–3.8 ka) within the Campi Flegrei caldera (southern Italy). *Lithos* 107:135–151
- Troise C, De Natale G, Pingue F, Obrizzo F, De Martino P, Tammaro U, Boschi E (2007) Renewed ground uplift at Campi Flegrei caldera (Italy): new insight on magmatic processes and forecast. *Geophys Res Lett* 34:L03301, 5PP. doi:[10.1029/2006GL028545](https://doi.org/10.1029/2006GL028545)
- Villemant B (1988) Trace element evolution in the Phlegraean Fields Central Italy: fractional crystallization and selective enrichment. *Contrib Mineral Petrol* 98:169–183
- Webster JD, Sintoni MF, De Vivo B (2009) The partitioning behavior of Cl, S, and  $\text{H}_2\text{O}$  in aqueous vapor-  $\pm$  saline-liquid saturated



- phonolitic and trachytic melts at 200 MPa. *Chem Geol* 263:19–36
- Wohletz K, Civetta L, Orsi G (1999) Thermal evolution of the Phlegraean magmatic system. *J Volcanol Geotherm Res* 91:381–414
- Zollo A, Maercklin N, Vassallo M, Dello Iacono D, Virieux J, Gasparini P (2008) Seismic reflections reveal a massive melt layer feeding Campi Flegrei caldera. *Geophys Res Lett* 35:L12306. doi:[10.1029/2008GL034242](https://doi.org/10.1029/2008GL034242)